

Constraints on the generalized natural inflation and reheating

Ya-Bo Wu,^{*} Nan Zhang,[†] Chu-Wen Sun, Li-Jie Shou, and Hai-Zhou Xu
Department of Physics, Liaoning Normal University, Dalian 116029, P.R.China
(Dated: December 14, 2024)

Based on the dynamics of single scalar field slow-roll inflation and the theory of reheating, we investigate the generalized natural inflationary (GNI) model. Concretely, by means of the observation data of scalar spectral index n_s and tensor-to-scalar ratio r , we firstly give constraints on the model parameters m and the e-folding number N_* corresponding to the different values of decay constant f . When taking $m = 1$, the model can reduce to the so-called natural inflationary (NI) model, and the allowable ranges of values of N_* and f can be obtained. By contrast, we find that $m < 1$ is well supported for a broad range of values of f . Next, for the general reheating phase characterized by the reheating e-folding number N_{re} , reheating temperature T_{re} and the effective average equation of state w_{re} , the physical conditions of $N_{re} \geq 0$ and $10^2 \text{ GeV} \leq T_{re} \leq 10^{16} \text{ GeV}$ can give more stringent constraints on the related parameters. The results show that the effect of f on the reheating phase is relatively weaker, in other words, these parameters are insensitive to the value of f , and the different values of w_{re} can lead to the significant changes to the parameters within the range of $-1 \leq w_{re} \leq 1$. Finally, we also discuss a two-phase reheating scenario consisting of the oscillation phase and the thermalization phase, and calculate the minimum coupling constant g in order to achieve the simplest two-phase reheating.

PACS numbers: 98.80.-k, 98.80.Cq, 98.80.Es

I. INTRODUCTION

Recent years, the areas of gravitational theory and cosmology attract much attention from the public. With the advances in technology and the increasing cross-cutting cooperations, we sketch the evolution picture of universe and know more about the mysterious dark sectors. However, many problems still remain uncertain, for example, no final conclusion has been reached on what is exactly the inflaton to generate the inflation phase in the very early universe.

Inflation is a widely accepted supplement to the standard big bang theory. The exist of inflation phase can lead to the universe experience a period of rapid accelerated expansion to solve the problems such as the flatness, the horizon, etc [1–5]. It can also give a superior interpretation of the origin of structure and cosmic microwave background (CMB) [6–8]. Then the cold and empty universe during inflation is heated through the reheating phase, the radiation particles corresponding to the standard model are also generated in the reheating epoch.

In order to investigate the properties of inflation period, many kinds of models have been proposed, such as hilltop models [9], natural inflation [10, 11], α attractors [12, 13] and so on. Most models are slow-roll ones taking a scalar field as the inflaton and making it slowly roll toward its true ground state [14–16].

As we know, the natural inflation (NI) model is a kind of single field slow-roll inflationary models. It was early researched in Refs. [10, 11] with the potential form as

$V(\phi) = \Lambda^4[1 \pm \cos(N\phi/f)]$, in which the choice of sign has no effect on the results, and usually, taking $N = 1$. The NI model is widely studied in many literatures because of its simple potential form and its theoretically well motivation [17–19]. It can naturally give rise to an epoch of inflation when the shift symmetry is spontaneously broken. The inflaton in the NI model is an axion or a pseudo-Nambu-Goldstone boson, which is also hot topic in Particle Physics.

Nevertheless, the NI model meets new challenges when considering the recent lower tensor-to-scalar ratio $r < 0.07$ released in Ref. [20] and the corresponding reheating stage. The tensor-to-scalar ratio r , together with scalar spectral index n_s , plays important role in fitting the model-dependent results of inflationary models with the observation data [21–24]. Besides, the behaviors of inflationary models are influenced by the e-folding number N_* and reheating e-folding number N_{re} , reheating temperature T_{re} and the effective average equation of state (EoS) w_{re} during reheating [25–27]. It means when discussing the behaviors of the inflationary models, we can use the combination of the above quantities to constrain the parameters of the models.

Since the NI model is not very well supported by the latest data but still well motivated, in this paper we focus on an inflationary model which was first proposed in Ref. [28], the authors added a power parameter m to the ordinary potential form in the NI model without loss of generality, i.e., $V(\phi) = 2^{1-m}\Lambda^4[1 + \cos(\frac{\phi}{f})]^m$. Here, we call this inflationary model as the generalized natural inflationary (GNI) model. Evidently, it can reduce to the NI model when $m = 1$. As we know, the e-folding number N_* , reheating e-folding number N_{re} and reheating temperature T_{re} have been calculated and discussed in Ref. [28], but the proper range of values of N_* were given only in the case of $m = 1$ according to the scalar spectral in-

^{*} ybwu61@163.com.

[†] zhangnandalian@163.com

dex n_s obtained by using the conditions of $T_{re} > 10^2$ GeV and $0 \lesssim w_{re} \lesssim 0.25$ [29]. Thus, it is an interesting issue how the parameter m in the GNI model to effect on the model behaviors and what ranges of values of the N_* , m and f can satisfy the requirements of observation. This is to say, we will try to investigate the constraints on the GNI model according to the observation data and give the tighter constraints on the related parameters by the physical conditions of the general reheating phase. On the other hand, we will also study a two-phase reheating process consisting of the oscillation phase and the thermalization phase by following the approach in Ref. [30]. Generally speaking, our motivation and purposes of this paper are investigating the constraints on the model parameters to show the validity of the GNI model and discuss its reheating scenario from two different perspectives.

Our research results indicate that the corresponding results to $m < 1$ are well supported by observation constraints. For the special case of $m = 1$, i.e., the NI model, the range of values of decay constant f is narrow. Moreover, we also calculate the running spectral index α_s as a supplement to the GNI model. Furthermore, when considering the general reheating phase, we find that the allowed regions for the parameters get smaller. Especially, for the two-phase reheating scenario, we calculate the coupling constant g and find that the requisite minimum values of g decreases first and then increases with the decay constant f .

This paper is organized as follows. In Sec. II, we briefly review the depiction of single scalar field slow-roll inflation and the theory of reheating epoch. In Sec. III, we give the information of parameters for the GNI model and investigate the constraints on the model based on the observation data from Planck and BICEP2/Keck Collaboration. Then we discuss the general reheating phase and the two-phase reheating for the GNI model. We give the more stringent constraints on the model parameters by using the physical conditions of the general reheating phase, and calculate the minimum coupling constant g for the successful simplest two-phase reheating. Sec. IV presents the conclusions.

II. SINGLE FIELD SLOW-ROLL INFLATION AND REHEATING

We will give a brief review how to constrain a single field inflationary model and its reheating phase. Following the approaches proposed in Refs. [30–32], we start with the equations of motion induced by a scalar field ϕ in the frame of spatially flat FRW background universe,

$$H^2 = \frac{1}{3M_p^2} \left(\frac{1}{2} \dot{\phi}^2 + V(\phi) \right), \quad (1)$$

$$\ddot{\phi} + 3H\dot{\phi} = -V'(\phi), \quad (2)$$

where $H \equiv \dot{a}/a$ is the Hubble parameter, $V(\phi)$ is the potential of field ϕ , $M_p \equiv \frac{1}{8\pi G} \simeq 2.435 \times 10^{18}$ GeV is the reduced Planck mass, the dot denotes differentiation with respect to cosmic time t and the prime denotes differentiation with respect to ϕ .

In the case of slow-roll inflation, the potential term dominates the total energy density and the scalar field changes slowly with time, the Eqs. (1) and (2) can be written as follows:

$$H^2 \simeq \frac{V(\phi)}{3M_p^2}, \quad (3)$$

$$3H\dot{\phi} \simeq -V'(\phi). \quad (4)$$

Thus, the parameter N_* , which represents the e-folding number between the pivot scale k_* exiting from the Hubble radius and the end of inflation, can be expressed in terms of the potential $V(\phi)$ under the slow-roll approximation

$$N_* \equiv \ln \frac{a_{end}}{a_*} = \int_{t_*}^{t_{end}} H dt \simeq -\frac{1}{M_p^2} \int_{\phi_*}^{\phi_{end}} \frac{V(\phi)}{V'(\phi)} d\phi, \quad (5)$$

where the subscript “*” and “end” correspond to crossing the horizon and the end of inflation, respectively.

Next, introducing the slow-roll parameters:

$$\epsilon_v = \frac{M_p^2}{2} \frac{V'(\phi)^2}{V(\phi)^2}, \quad (6)$$

$$\eta_v = M_p^2 \frac{V''(\phi)}{V(\phi)}, \quad (7)$$

$$\xi_v^2 = M_p^4 \frac{V'(\phi)V'''(\phi)}{V(\phi)^2}, \quad (8)$$

then the scalar spectral index n_s , its running α_s and the tensor-to-scalar ratio r can be expressed as:

$$n_s \simeq 1 - 6\epsilon_v + 2\eta_v, \quad (9)$$

$$\alpha_s \equiv \frac{dn_s}{d \ln k} \simeq 16\epsilon_v\eta_v - 24\epsilon_v^2 - 2\xi_v^2, \quad (10)$$

$$r \simeq 16\epsilon_v. \quad (11)$$

As for the reheating phase, the starting point is the relation $k = aH$. It leads to:

$$\begin{aligned} 0 &= \ln \frac{a_{end}}{a_*} + \ln \frac{a_{re}}{a_{end}} + \ln \frac{a_0}{a_{re}} + \ln \frac{k_*}{a_0 H_*} \\ &= N_* + N_{re} + \ln \frac{a_0}{a_{re}} + \ln \frac{k_*}{a_0 H_*}, \end{aligned} \quad (12)$$

where the subscript “re” corresponds to the end of reheating, a_0 means the present value of scale factor

which is equal to 1, k_* is chosen to be 0.05 Mpc^{-1} . Based on the conservation of entropy density $g_{re} a_{re}^3 T_{re}^3 = g_\gamma a_0^3 T_\gamma^3 + \frac{7}{8} g_\nu a_0^3 T_\nu^3$ and the relationship of temperature $T_\nu/T_\gamma = (4/11)^{1/3}$, the expression of a_{re}/a_0 can be written as $a_{re}/a_0 = (43/11g_{re})^{1/3}/(T_\gamma/T_{re})$, $T_\gamma = 2.7255 \text{ K}$ is a known quantity. The subscripted parameter g is the effect number of degrees of freedom, $g_\gamma = 2$ and $g_\nu = 6$, g_{re} is assuming as 10^3 for single scalar field inflationary models in keeping with *Planck* 2015 [24, 33].

Considering the energy density of the Universe at the end of the reheating $\rho_{re} = g_{re} \frac{\pi^2}{30} T_{re}^4$ and the continuity equation $\rho_{re} = \rho_{end} \exp[-3(1+w_{re})N_{re}]$, the expression of temperature at the end of reheating can be obtained,

$$T_{re} = \exp\left[-\frac{3}{4}(1+w_{re})N_{re}\right] \left(\frac{45V_{end}}{g_{re}\pi^2}\right)^{1/4}, \quad (13)$$

where w_{re} is regarded as the average EoS during reheating, V_{end} is used to substitute for ρ_{end} [33]. The relation between V_{end} and ρ_{end} can be deduced by taking $\epsilon_H = \frac{3}{2}(1+w) = \epsilon_{end}$, and $\epsilon_{end} = 1$ is the sign of the end of inflation. $\epsilon_H \equiv -\dot{H}/H^2$ is the first Hubble hierarchy parameter, in slow-roll approximation, $\epsilon_H \simeq \epsilon_v$. For a scalar field, $w \equiv P/\rho = \frac{\frac{1}{2}\dot{\phi}^2 - V}{\frac{1}{2}\dot{\phi}^2 + V}$. After a simple calculation, we can get $\rho_{end} \simeq \frac{3}{2}V_{end}$. Hence, the third term on the righthand in Eq. (12) can be rewritten as $\ln \frac{a_0}{a_{re}} = \frac{1}{3} \ln \frac{11g_{re}}{43} - \frac{3}{4}(1+w_{re})N_{re} + \frac{1}{4} \ln \frac{45V_{end}}{g_{re}\pi^2} - \ln T_\gamma$. Therefore, H_* is the only uncertain quantity in Eq. (12) and it can be fixed by combining Eq. (3) with the equation of scalar power spectrum amplitude $A_s \simeq H_*^2/(\pi^2 M_p^2 r/2)$, $\ln[10^{10} A_s]$ is equal to 3.094 ± 0.034 for *Planck* TT,TE,EE+lowP [24]. In this paper, the central value 3.094 is adopted.

Finally, the expression of the e-folding number N_{re} during reheating can be written as follows:

$$N_{re} = \frac{4}{1-3w_{re}} \left[-N_* - \frac{1}{3} \ln \frac{11g_{re}}{43} - \frac{1}{4} \ln \frac{45V_{end}}{g_{re}\pi^2} - \ln \frac{k_*}{T_\gamma} + \frac{1}{2} \ln(\pi^2 M_p^2 (r/2) A_s) \right]. \quad (14)$$

III. THE GENERALIZED NATURAL INFLATIONARY MODEL

As we know, the ordinary NI potential was simply generalized by adding one parameter m in Ref. [28], here we call this model as the generalized natural inflationary (GNI) model. The form of potential for the GNI model is expressed as follows:

$$V(\phi) = 2^{1-m} \Lambda^4 \left[1 + \cos\left(\frac{\phi}{f}\right) \right]^m, \quad (15)$$

where the energy density Λ^4 , decay constant f and the constant m are the parameters of the model. It follows that when $m = 1$, it can reduce to the so-called NI model. If $f \rightarrow \infty$, the NI model seems to behave like the chaotic

inflationary model. Similarly, the GNI model behaves as a pure power law model when $f \rightarrow \infty$ [28].

It should be noted that for the NI model, only lower limit of f , namely, $f \gtrsim 0.3M_p$ exists in the primary literature Ref. [11]. Although *Planck* 2015 favors the NI model with a new lower bound as $\lg(f/M_p) > 0.83$ for $w_{re} = 0$ (allowing w_{re} to vary), the values below this scale still can not be simply excluded under some suitable choices [24]. For example, in Ref. [17], the bound on $\lg(f/M_p)$ is slightly loosened by making use of the reheating phase diagrams for the NI model in the $N_{re} - w_{re}$ plane. Thus, we will need to investigate the GNI model with a broad range of values of f .

Fig. 1 shows the evolving tendency of the potential

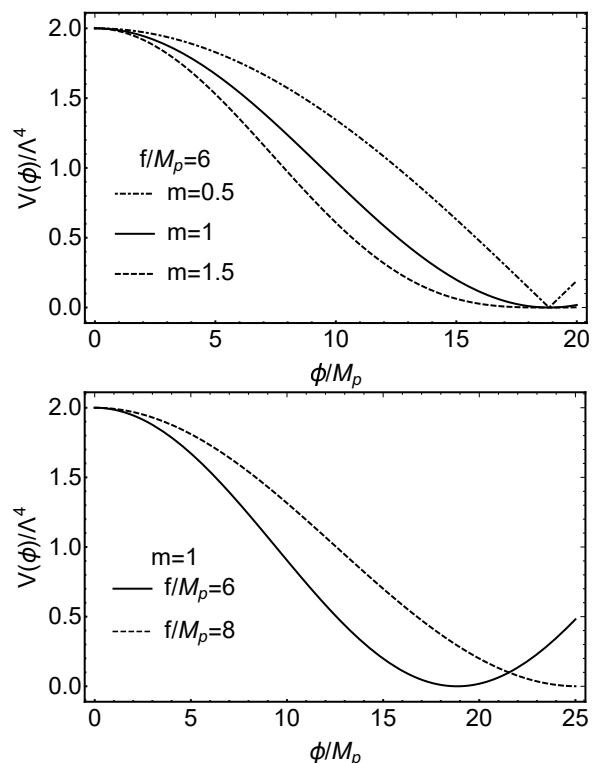


FIG. 1. The evolving trajectories of $V(\phi)$ in the GNI model.

roughly. The horizontal axis is ϕ/M_p , the vertical axis is $V(\phi)/\Lambda^4$. From the trajectories, we can find that if f is a fixed value, such as $f/M_p = 6$ in the upper panel, $V(\phi)$ changes more slowly for smaller m in the beginning and becomes steep in the end, the trajectories reach zero at the same value of ϕ . For the fixed m , for example, taking $m = 1$ in the lower panel, the bigger the value of f , the slower the change of $V(\phi)$.

A. The constraints on parameters in the GNI model

According to Eqs. (6) and (7), the slow-roll parameters ϵ_v and η_v for GNI model can be given as follows:

$$\epsilon_v = \frac{M_p^2 m^2}{2f^2} \left[\frac{1 - \cos(\phi/f)}{1 + \cos(\phi/f)} \right], \quad (16)$$

$$\eta_v = -\frac{M_p}{f^2} \left[\frac{m - m^2(1 - \cos(\phi/f))}{1 + \cos(\phi/f)} \right]. \quad (17)$$

Thus, n_s and r can be expressed as:

$$n_s = 1 - \frac{M_p^2}{f^2} \left[\frac{m^2(1 - \cos(\phi/f) + 2m)}{1 + \cos(\phi/f)} \right], \quad (18)$$

$$r = \frac{8M_p^2 m^2}{f^2} \left[\frac{1 - \cos(\phi/f)}{1 + \cos(\phi/f)} \right]. \quad (19)$$

And the e-folding number N_* is derived as:

$$N_* = \frac{f^2}{mM_p^2} \ln \frac{1 - \cos(\phi_{end}/f)}{1 - \cos(\phi_*/f)}. \quad (20)$$

When $\epsilon_v = \epsilon_{end} = 1$, ϕ_{end} can be obtained from Eq. (16) as follows

$$\phi_{end} = f \arccos \frac{m^2 M_p^2 - 2f^2}{m^2 M_p^2 + 2f^2}. \quad (21)$$

Substituting Eq. (21) into Eq. (20), ϕ_* can be derived as

$$\phi_* = f \arccos \left[1 - \frac{4f^2}{m^2 M_p^2 + 2f^2} \exp\left(-\frac{mM_p^2}{f^2} N_*\right) \right]. \quad (22)$$

It follows that ϕ_* is the function of (f, N_*, m) . In this case, Eqs. (18) and (19) become into

$$n_s = 1 - \frac{mM_p^2}{f^2} \left[1 + \frac{2f^2(m+1) \exp\left(-\frac{mM_p^2}{f^2} N_*\right)}{m^2 M_p^2 + 2f^2(1 - \exp\left(-\frac{mM_p^2}{f^2} N_*\right))} \right], \quad (23)$$

$$r = \frac{16m^2 M_p^2 \exp\left(-\frac{mM_p^2}{f^2} N_*\right)}{m^2 M_p^2 + 2f^2(1 - \exp\left(-\frac{mM_p^2}{f^2} N_*\right))}. \quad (24)$$

It is easy to see that when taking $m = 1$, Eqs. (18) and (19) can reduce to the results in the NI model. As we know, the widely accepted data of n_s and r are given by *Planck* 2015 as $n_s = 0.9652 \pm 0.0047$ (68% CL, *Planck* TT,TE,EE+lowP) for Λ CDM + r , at 95% CL, $n_s = 0.9652^{+0.0093}_{-0.0091}$ and $r < 0.106$ at pivot scale $k_* = 0.05 \text{ Mpc}^{-1}$ [24]. Later in 2016, the upper limit of r decreases to $r < 0.07$ by the *Planck* data together with the BICEP2/Keck data [20]. Here, we will adopt

$0.9561 \leq n_s \leq 0.9745$ and $r < 0.07$ as the observation constraints.

In what follows in Fig. 2, we plot the allowable ranges of values of N_* and m , for the fixed values of f , by means of the observation data. The horizontal axis is N_* with the general reasonable range of values $40 \leq N_* \leq 70$, the vertical axis is m with the appropriate range of values. In each panel of the figure, the solid and dashed lines respectively represent the boundaries of the satisfied region for n_s and r . The shaded region just exhibits the allowable region for N_* and m . The dotted lines correspond to the case of $m = 1$. Note that only some typical cases are shown in the figure to save some space.

From Fig. 2, we find that the region surrounded by dashed lines becomes smaller with increasing f , while the region surrounded by solid lines shows a contrary tendency. It means that the ranges of values of the parameters N_* and m are more determined by n_s for smaller f , but when $f > 5M_p$, they are more determined by r . Meanwhile, the maximum of m becomes bigger with increasing f until $f = 8M_p$, after that, it becomes smaller. When $f \gtrsim 13M_p$, the upper limit to N_* becomes smaller as the value of f increases. (See Table I). Hence, a significant conclusion can be drawn that $m < 1$ is supported for a broad range of values of f , and the appearing maximum of m is $m = 2.11$.

Similarly, Fig. 3 shows the allowed ranges of values of N_* and f when taking $m = 0.5, 1$ and 1.5 , respectively. Evidently, the so-called NI model corresponds to the case of $m = 1$ in the middle panel. According to Fig. 3, the shaded region apparently becomes smaller with increasing m , which indicates that the parameter m indeed has an effect on the parameter space for the GNI model. In particular, it is worth stressing that, for the NI model corresponding to $m = 1$, there exists the constraints on the parameters of N_* and f , i.e., $N_* > 52.18$ and $5.10 \leq f/M_p \leq 8.85$. If $m > 1$, the observation data leads to smaller ranges of values of N_* and f than the ones in the NI model, for example, $N_* > 60.5$ and $6.42 \leq f/M_p \leq 8.22$ for $m = 1.5$ (see the right panel in Fig. 3). But in the case of $m < 1$, as noted above, will give a larger parameter space than the case of $m = 1$. In the case of $m = 0.5$, see the left panel in Fig. 3, a lower bound on f is $f/M_p \geq 3.53$. The range of values of N_* is also relaxed to $40 \leq N_* \leq 70$, although more values of f will be supported when the values of N_* lie in the middle range of values. For example, if $f/M_p = 20$, the range of values of N_* is $54.9 \leq N_* \leq 59.3$ when taking $m = 0.5$.

Moreover, we can calculate the higher-order third slow-roll parameter ξ_v^2 and the running spectral index α_s based on Eqs. (8), (10) and (22) as follows:

$$\xi_v^2 = m^2 M_p^4 \frac{4f^2 m^2 - (3m-1)(2f^2 + m^2 M_p^2) e^{\frac{mM_p^2}{f^2} N_*}}{(-2f^3 + (2f^3 + fm^2 M_p^2) e^{\frac{mM_p^2}{f^2} N_*})^2}, \quad (25)$$

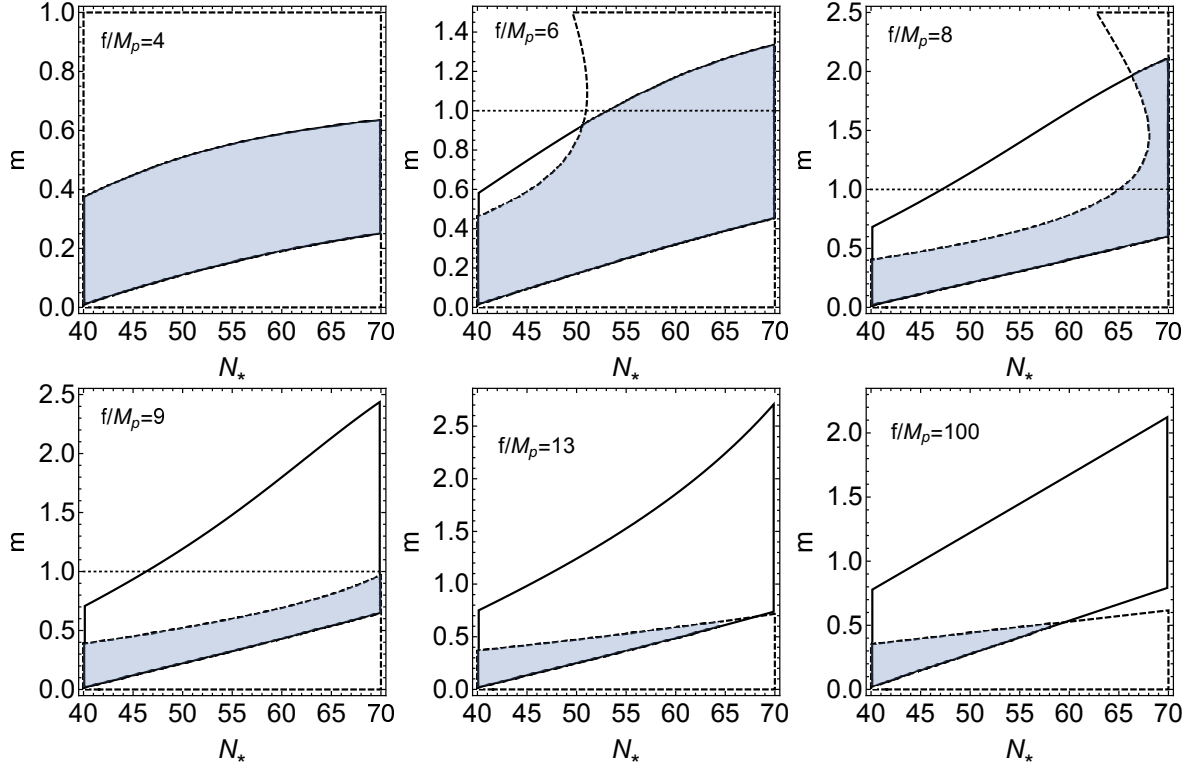


FIG. 2. Allowed ranges of values of N_* and m for the different values of f . In each panel, the solid curves bracket the range of values $0.9561 \leq n_s \leq 0.9745$, the dashed curves bracket the range of values $r < 0.07$, and the shaded region is their intersection.

TABLE I. Allowed ranges of values of N_* and m for the different values of f .

f/M_p	1	2	3	4	5	6	7	8
m	0.001 – 0.04	0.003 – 0.16	0.01 – 0.36	0.01 – 0.63	0.01 – 0.96	0.01 – 1.34	0.01 – 1.73	0.02 – 2.11
N_*	40 – 70	40 – 70	40 – 70	40 – 70	40 – 70	40 – 70	40 – 70	40 – 70
f/M_p	9	10	11	12	13	14	15	20
m	0.02 – 0.97	0.02 – 0.84	0.02 – 0.78	0.02 – 0.74	0.02 – 0.69	0.02 – 0.65	0.02 – 0.63	0.02 – 0.57
N_*	40 – 70	40 – 70	40 – 70	40 – 70	40 – 68.10	40 – 66.23	40 – 64.98	40 – 62.12
f/M_p	30	40	50	60	70	80	90	100
m	0.02 – 0.54	0.02 – 0.53	0.02 – 0.53	0.02 – 0.53	0.02 – 0.53	0.02 – 0.52	0.02 – 0.52	0.02 – 0.52
N_*	40 – 60.53	40 – 60.04	40 – 59.82	40 – 59.70	40 – 59.63	40 – 59.59	40 – 59.56	40 – 59.53

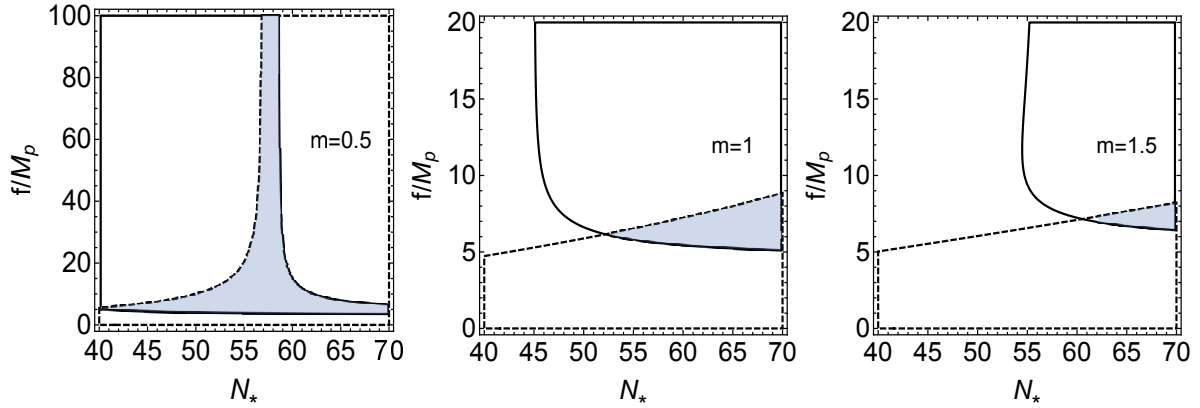


FIG. 3. Allowed ranges of values of N_* and f for the different values of m . In each panel, the solid curves bracket the range of values $0.9561 \leq n_s \leq 0.9745$, the dashed curves bracket the range of values $r < 0.07$, the shaded region is their intersection.

$$\alpha_s \simeq \frac{-2m^2(m+1)M_p^4(2f^2 + m^2M_p^2)e^{\frac{mM_p^2}{f^2}N_*}}{-2f^3 + (2f^2 + m^2M_p^2) + e^{\frac{mM_p^2}{f^2}N_*}}. \quad (26)$$

In Fig. 4, we plot α_s with respect to variables N_* and m corresponding to $f/M_p = 4, 6$ and 9 , respectively. The numbers marked on the solid contour curves are the values of α_s . The shaded regions represent the allowed regions for observation data, which are consistent with the corresponding case in Fig. 3. It can be seen that the value of α_s increases with N_* , however, it changes complexly with m . In the first two panels, α_s decreases first and then increases with increasing m . We give the ranges of values of α_s for different values of f and find that the ranges are almost same for large values of f . (see Table II).

TABLE II. Allowed ranges of values of α_s for the different values of f .

f/M_p	α_s
1	-0.00062 \sim -0.00011
2	-0.00063 \sim -0.00013
3	-0.00070 \sim -0.00015
4	-0.00079 \sim -0.00018
5	-0.00087 \sim -0.00022
6	-0.00088 \sim -0.00027
7	-0.00087 \sim -0.00030
8	-0.00070 \sim -0.00015
9	-0.00086 \sim -0.00032
10	-0.00085 \sim -0.00033
11	-0.00085 \sim -0.00034
12	-0.00085 \sim -0.00035
13	-0.00085 \sim -0.00036
14	-0.00085 \sim -0.00037
15	-0.00085 \sim -0.00038
20	-0.00085 \sim -0.00040
30	-0.00084 \sim -0.00042
40	-0.00084 \sim -0.00042
50	-0.00084 \sim -0.00042
60	-0.00084 \sim -0.00043
70	-0.00084 \sim -0.00043
80	-0.00084 \sim -0.00042
90	-0.00084 \sim -0.00042
100	-0.00084 \sim -0.00043

B. The general reheating phase for the GNI model

For general reheating epoch, substituting the expressions of V_{end} and r into Eqs. (13) and (14), N_{re} and T_{re} can be obtained for the GNI model.

As we know, rapid accelerated expansion of the universe during inflation requires the EoS $w < -1/3$ and the EoS of radiation is $w = 1/3$. Therefore, the range of effect average values of EoS during the reheating period is often regarded as $w_{re} \in [-1/3, 1/3]$. But from the view of scalar field, when the energy density and pressure of

the scalar field inflaton are dominated by the potential energy, its EoS approximates to $w = -1$, and $w = 1$ corresponds to the case of kinetic energy dominated. Hence, we could here assume a broader range of values, i.e., $w_{re} \in [-1, 1]$. In addition, since the physical mechanism of reheating has been uncertain, the complexity of the thermodynamics would lead to a higher EoS than the one of radiation era.

It is easy to find the denominator of Eq. (14) will vanish if $w_{re} = 1/3$. Hence the value of $w_{re} = 1/3$ is the boundary of different evolution of tendencies for reheating parameters. We illustrate the evolving trajectories of the reheating e-folding number N_{re} and the reheating temperature T_{re} in Fig. 5.

We take $w_{re} = -1/3$ as the example of $w_{re} < 1/3$ and $w_{re} = 1$ is the representative of $w_{re} > 1/3$. Evidently, when $w_{re} < 1/3$, N_{re} becomes smaller and T_{re} becomes higher with the increasing N_* . In the case of $w_{re} > 1/3$, they change in the opposite trends. The upper panels in Fig. 5 show the influence of f on N_{re} and T_{re} when $m = 0.5$. The almost overlapping curves suggest that N_{re} and T_{re} is insensitive to the value of f . By contrast, the lower panels illustrate the changes of N_{re} and T_{re} with m when taking $f = 6M_p$. In the case of $w_{re} < 1/3$, the smaller the value of m , the smaller the value of N_{re} and the larger the value of T_{re} , while in the case of $w_{re} > 1/3$, the results are opposite.

We know that the reheating e-folding number N_{re} should be positive in order to make the reheating phase physically meaningful. On the other hand, the reheating temperature T_{re} should be higher than the electro-weak energy scale 10^2 GeV and lower than the grand unification scale 10^{16} GeV. Therefore, below, we will give further constraints on the parameters of the GNI model by the physical conditions of the general reheating phase, i.e., $N_{re} \geq 0$ and $10^2 \text{ GeV} \leq T_{re} \leq 10^{16} \text{ GeV}$.

In Fig. 6, we plot the restricted regions in $N_* - m$ plane corresponding to $w_{re} = -1, -\frac{1}{3}, 0, \frac{1}{4}, \frac{2}{5}$ and 1 respectively. Due to the insensitiveness of the parameters to f , we chose a fixed value of f , for example, $f/M_p = 6$. The solid curves bracket the ranges of values $N_{re} \geq 0$ and the dashed curves bracket the ranges of values $10^2 \text{ GeV} \leq T_{re} \leq 10^{16} \text{ GeV}$. Thus, the grid-shadow regions are theoretically the allowed ranges of values of N_* and m satisfying the physical conditions of the general reheating. The shaded regions correspond to the allowed ranges of values of N_* and m constrained by the observation data. That is to say, the overlaps between the shaded regions and grid-shadow regions are the final allowed ranges of values of N_* and m when taking $f/M_p = 6$, which are just the results imposed by the reheating conditions and observational data. Obviously, the allowed areas decrease first and then increase with the increasing of w_{re} .

Moreover, we find that there are the maximum and minimum of N_* for the cases of $w_{re} < 1/3$ and $w_{re} > 1/3$, respectively, i.e., $N_*^{max} = 56.86$ and $N_*^{min} = 56.01$. Evidently, the physical conditions of the general reheating phase can further decrease the allowed ranges of values

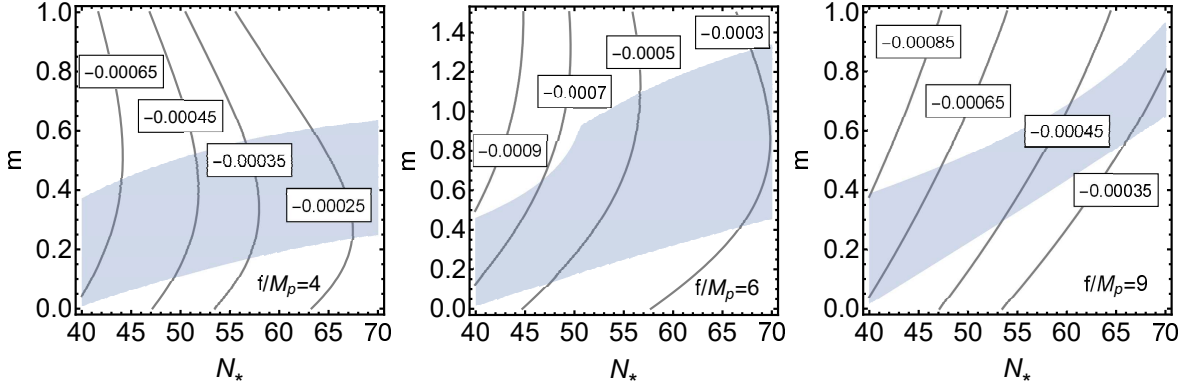


FIG. 4. The running scalar spectral index α_s with respect to variables N_* and m according to $f/M_p = 4, 6$ and 9 , respectively. The shaded region in each panel is the allowed region for observation data.

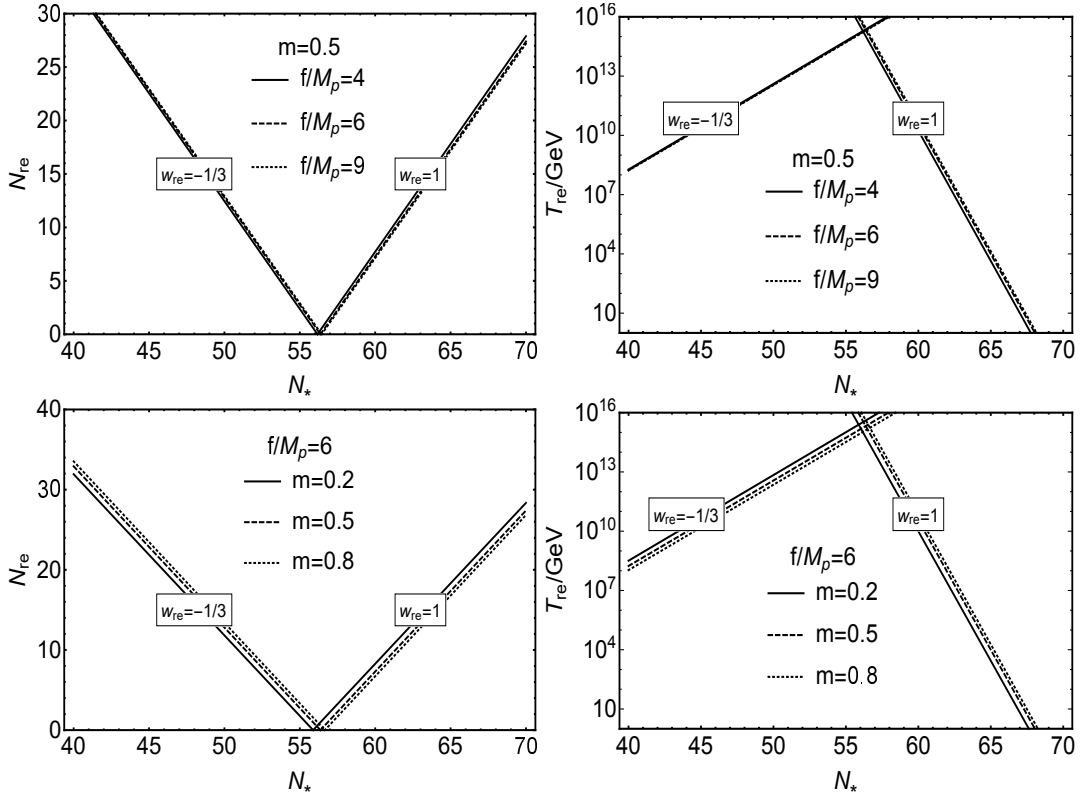


FIG. 5. The evolving trajectories of the reheating e-folding number N_{re} and the reheating temperature T_{re}/GeV with N_* .

of N_* and m for a fixed value of f , such as the range of values of N_* is $40 \leq N_* \leq 66.88$ and the maximum of m is 1.29 when taking $f/M_p = 6$. The concrete results of the allowed ranges of values of N_* and m and the corresponding ranges of values of N_{re} and the order of magnitude of T_{re}/GeV are listed in Table III.

It is easy to see that the global maximum of N_{re} is about 40 appearing at $w_{re} = 0$, and value of maximum of N_{re} first increases and then decreases with the increasing w_{re} . The reheating temperature has a broad range of values when $w_{re} \geq 0$, it is at the higher scale when $w_{re} < 0$, for example, T_{re} should be higher than $1.9 \times 10^8 \text{ GeV}$

for $w_{re} \leq -1/3$.

C. The two-phase reheating for the GNI model

Below we consider the reheating scenario as a simple case of two-phase process. After the end of inflation, scalar field inflaton starts to oscillate and decay into radiation field χ which is the so-called oscillation phase. At the equal scale, when the energy density of the oscillation field equals to the one of relativistic particle field, i.e., the expansion Hubble constant H equals to the decay

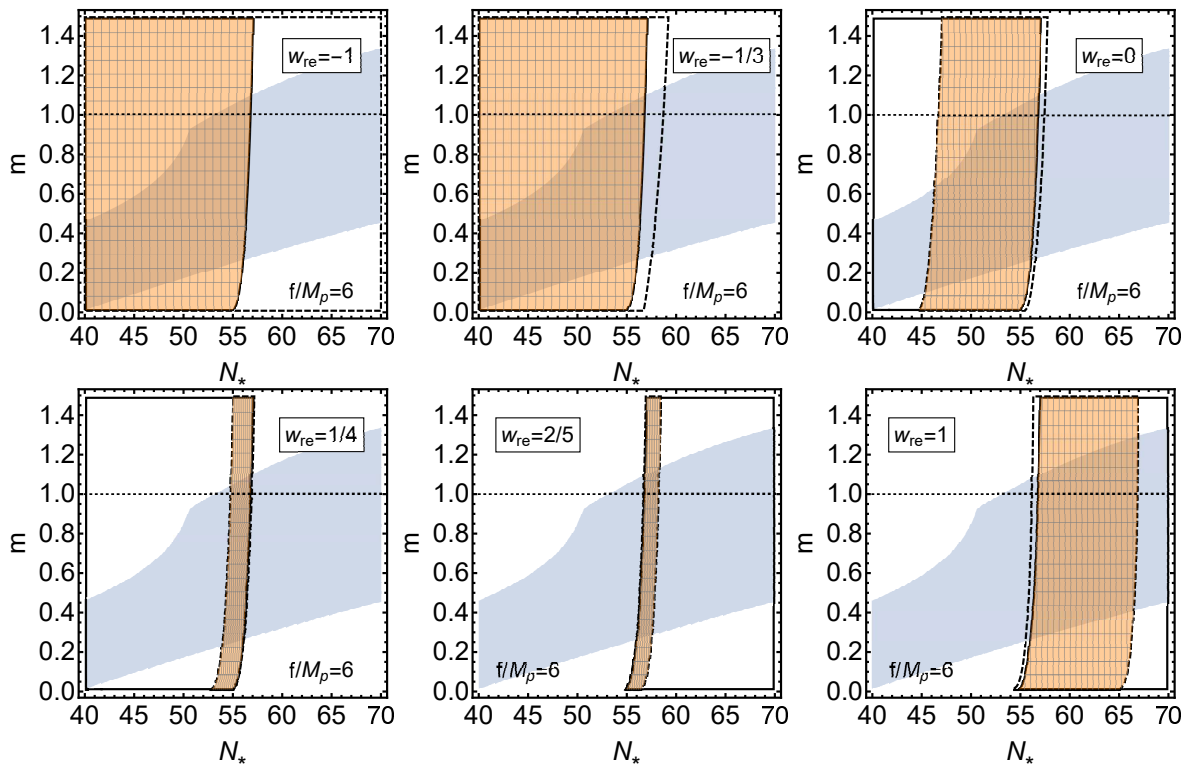


FIG. 6. Allowed ranges of values of N_* and m for the different values of w_{re} when $f/M_p = 6$. In each panel, the solid curves bracket the range of values $N_{re} \geq 0$, the dashed curves bracket the range of values $10^2 \text{ GeV} \leq T_{re} \leq 10^{16} \text{ GeV}$, the grid-shadow region is their intersection, the shaded region is the allowed region for the observation data.

TABLE III. Allowed value ranges of N_* and m , and the corresponding value ranges of N_{re} and T_{re}/GeV for $f/M_p = 6$.

w_{re}	N_*	m	N_{re}	T_{re}/GeV
-1	40.00 – 56.86	0.01 – 1.10	0 – 16.40	$1.4 \times 10^{15} - 2.8 \times 10^{15}$
-1/3	40.00 – 56.86	0.01 – 1.10	0 – 32.80	$1.9 \times 10^8 - 2.4 \times 10^{15}$
0	45.35 – 56.86	0.10 – 1.10	0 – 41.18	$10^2 - 2.5 \times 10^{15}$
1/4	53.90 – 56.86	0.23 – 1.10	0 – 32.91	$10^2 - 2.5 \times 10^{15}$
2/5	56.01 – 58.30	0.26 – 1.13	0 – 29.43	$10^2 - 2.3 \times 10^{15}$
1	56.01 – 66.88	0.26 – 1.29	0 – 20.45	$10^2 - 2.4 \times 10^{15}$

rate Γ , the universe is going to be dominated by radiation. Therefore, $H = \Gamma$ is regarded as the sign of completing the simplest two-phase reheating. Note that, the system is not at thermal equilibrium during the process, and it has gone through a process called thermalization phase. When the ϕ field oscillates around its minimum value, the potential Eq. (15) has an approximate form of $V(\phi) \propto \phi^{2m}$. For the ϕ^{2m} form-like potential, the EoS can be expressed as [30, 34]:

$$w_{sc} = \frac{m-1}{m+1}. \quad (27)$$

The reheating e-folding number N_{re} is reconsidered as the sum of two phases, N_{sc} and N_{th} . We know that $N_{sc} = \ln \frac{a_{eq}}{a_{end}}$ and $N_{th} = \ln \frac{a_{re}}{a_{eq}}$, where a_{eq} is the dividing

point of the two phases. They can be written as

$$N_{sc} = -\frac{1}{3(1+w_{sc})} \ln \frac{\rho_{eq}}{\rho_{end}}, \quad (28)$$

and

$$N_{th} = -\frac{1}{4} \ln \frac{\rho_{re}}{\rho_{eq}}, \quad (29)$$

where $w_{th} = w_r = 1/3$ has been adopted in Eq. (29).

Based on the continuity equation, ρ_{eq} can be expressed as

$$\begin{aligned} \rho_{eq} &= \rho_{end} \exp[-3(1+w_{sc})N_{sc}] \\ &= \frac{3}{2} V_{end} \exp[-3(1+w_{sc})N_{sc}]. \end{aligned} \quad (30)$$

Finally, Eqs. (28) and (29) can be rewritten as follows:

$$N_{sc} = \frac{4}{1-3w_{sc}} \left[-N_* - \frac{1}{3} \ln \frac{11g_{re}}{43} - \frac{1}{4} \ln \frac{45V_{end}}{g_{re}\pi^2} - \ln \frac{k_*}{T_\gamma} + \frac{1}{2} \ln \frac{\pi^2 M_{pl}^2 r A_s}{2} \right], \quad (31)$$

$$T_{re} e^{N_{th}} = \exp \left[-\frac{3}{4} (1+w_{sc}) N_{sc} \right] \left(\frac{45V_{end}}{g_{re}\pi^2} \right)^{1/4}. \quad (32)$$

Fig. 7 shows the relations of oscillation e-folding number N_{sc} and the temperature $T_{re} e^{N_{th}} / \text{GeV}$ with N_* for fixed values of m and f . We find N_{sc} is decreasing, while $T_{re} e^{N_{th}}$ is increasing with N_* . Similar to the cases of general reheating phase, they are insensitive to the value of f , but the value of m has evident influence on them.

In Fig. 8, the values of N_{sc} and $T_{re} e^{N_{th}} / \text{GeV}$ are drawn by solid curves with respect to variables N_* and m for the case of $f/M_p = 6$, the shaded regions represent the allowable ones constrained by the observation data. The requirement of a physical meaningful oscillation phase is $N_{sc} \geq 0$. The dashed line in the right panel corresponds to $N_{sc} = 0$, which means the region in the right side of the dashed line is unphysical as it corresponds to $N_{sc} < 0$. The maximum of N_{sc} is about 30, and $3.2 \times 10^9 \text{ GeV} \leq T_{re} e^{N_{th}} \leq 2.5 \times 10^{15} \text{ GeV}$.

In addition, we consider the elementary decay $\phi \rightarrow \chi\chi$ with the interaction $-g\phi\chi^2$, where g respects the coupling constant. And following Ref. [30], we take the corresponding decay rate Γ as $\Gamma_{\phi \rightarrow \chi\chi} = \frac{g^2}{8\pi m_\phi}$, where m_ϕ is the mass of inflaton. Considering the Friedmann Equation $H^2 = \frac{\rho_{eq}}{3M_p^2}$ and the equality of $H = \Gamma$, it can be directly obtained that $(\frac{\rho_{eq}}{3M_p^2})^{1/2} = \frac{g^2}{8\pi m_\phi}$. Substituting Eqs. (27) and (30) into the above equation, the coupling constant g for the GNI model can be deduced as follows:

$$g = \sqrt{\frac{8\pi m_\phi}{M_p} \left(\frac{V_{end}}{2} \right)^{1/4}} \exp \left[-\frac{3m}{2(m+1)} N_{sc} \right]. \quad (33)$$

Utilizing $V_{end} \sim 2^{1-m} \Lambda^4 \left(\frac{mM_p}{f} \right)^{2m}$, the effective mass of inflaton ϕ at vacuum $m_\phi^2 \sim m \frac{\Lambda^4}{f^2}$ and Eq. (31), g can be expressed in terms of (f, N_*, m) . Therefore, when taking the different values of f , we can give the minimum values of coupling constant g to realize a successful simplest two-phase reheating scenario.

In Fig. 9, we plot the coupling constant g with respect to variables N_* and m for $f/M_p = 4, 6$ and 9 as examples. Similar to Fig. 8, the shaded regions are the allowable ones constrained by the observation data, the dashed lines correspond to $N_{sc} = 0$ for the given values of f , and the regions left to the dashed lines are valid due to the physical condition of $N_{sc} \geq 0$.

From Fig. 9, we find that the value of g increases with N_* , but decreases with m . It can be seen that the maximum of g is slightly less than 10^{14} GeV , and the

minimum of g for the different values of f are listed in the form of $\lg(g / \text{GeV})$ in Table IV.

We can conclude that the minimum of g decreases first and then increases with f . The minimum of g should be higher than 10^7 GeV for different values of f . It is easy to see when f is large enough, the minimum of g is almost unchanged.

IV. CONCLUSIONS

In summary, in the paper we have in detail investigated the generalized natural inflationary (GNI) model and its reheating phase. For the GNI model with the potential form in Eq. (15), the observables n_s and r have been expressed by N_* , m and f . If taking $m = 1$, it can reduce to the case of the natural inflationary (NI) model.

As we discussed above, the allowed ranges of values of N_* and m for different values of f have been illustrated in Fig. 2 and Table I by means of the observation data of $0.9561 \leq n_s \leq 0.9745$ and $r < 0.07$. Moreover, when considering the general reheating phase, the results are insensitive to the value of f and the ranges of values of N_* and m have been tightened for a fixed value of f , for example, $f/M_p = 6$. (see Fig. 6 and Table III). Furthermore, we have also calculated the running index α_s and the coupling constant g in the case of the two-phase reheating.

Our new results for the GNI model are concluded as follows:

(i) The model parameter m has significant effect on the validity of the model. If taking $m < 1$, the ranges of values of f/M_p and N_* are broader than the ones in the NI model. In other words, $m < 1$ is well supported by the observation data. Conversely, $m \geq 1$ dramatically narrows the allowed ranges of these values. It is also worth noting that when taking $m = 1$, the range of values of f is smaller than the one in Ref. [17] according to the recent data of $r < 0.07$.

(ii) The allowed ranges of values of N_* and m have been more stringently constrained by the physical conditions of general reheating phase for a fixed value of f/M_p . As we have shown above, the value of f has little effect on the results of the general reheating phase. And the value of w_{re} primarily affects the available ranges of values of N_* and m . If the same assumption of $0 \lesssim w_{re} \lesssim 1/4$ is adopted as the one in Ref. [28], N_* could be in the range of values of $53.21 \leq N_* \leq 56.80$ when taking $f/M_p = 6$ for the NI model corresponding to $m = 1$. Meanwhile, the maximum of m could be smaller than 2. Evidently, comparing with the values in Ref. [28], the minimum of N_* becomes big and the maximum of m becomes small.

(iii) Instead of w_{re} , in the case of the two-phase reheating scenario, the important parameter is w_{sc} , which is expressed as the function of m . The results here are still insensitive to the value of f . In addition, the lowest strength of coupling constant g is about 10^7 GeV for realizing the successful simplest two-phase reheating.

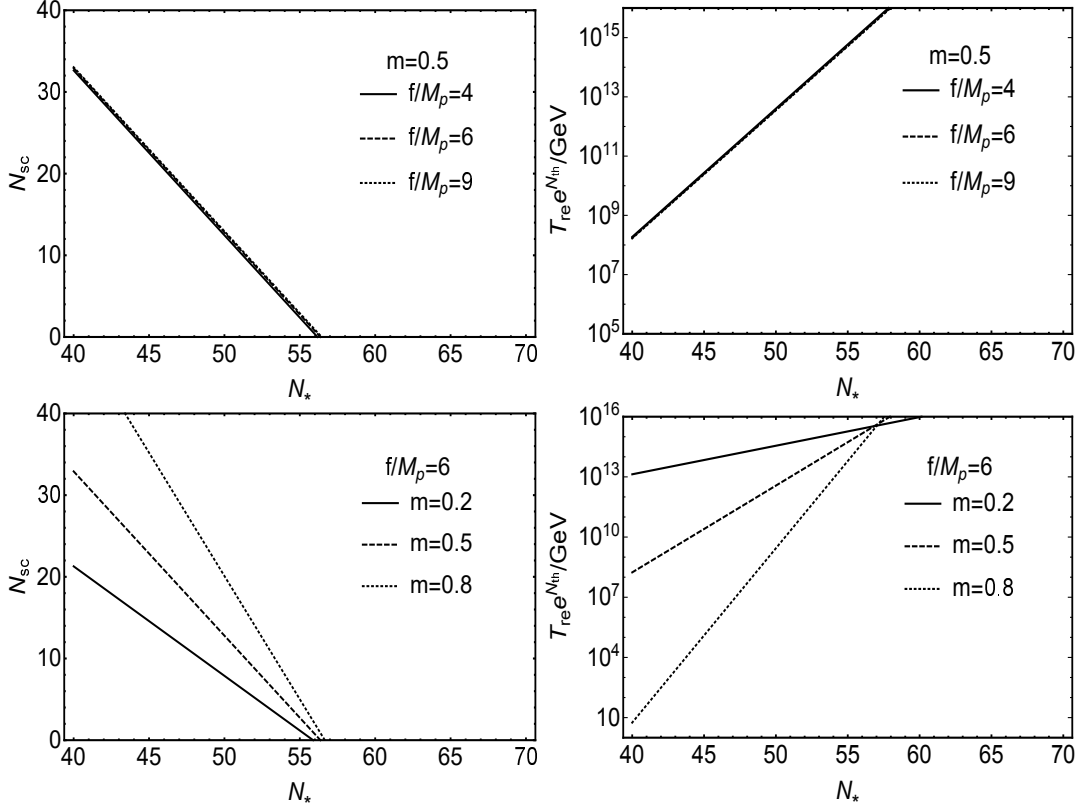


FIG. 7. The evolving trajectories of the oscillation e-folding number N_{sc} and the reheating temperature T_{re}/GeV timing $e^{N_{th}}$ with N_* in the two-phase reheating scenario.

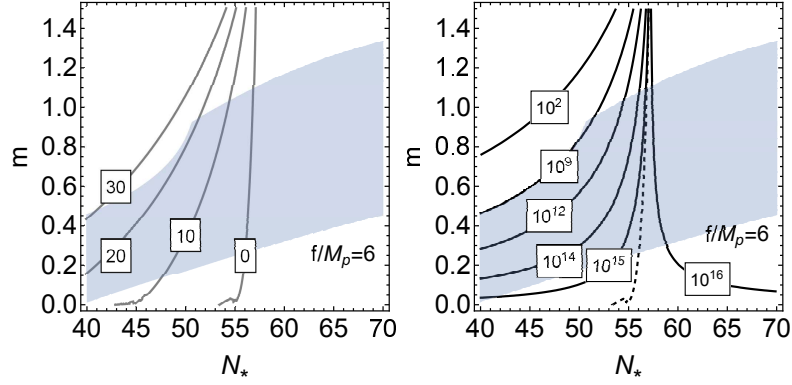


FIG. 8. The values of N_{sc} and $T_{re}e^{N_{th}}/\text{GeV}$ with respect to variables N_* and m in the two-phase reheating scenario. Here, we chose $f/M_p = 6$.

TABLE IV. The values of minimum of $\lg(g/\text{GeV})$ for the different values of f .

f/M_p	1	2	3	4	5	6	7	8	9	10	11	12
$\lg(g/\text{GeV})^{min}$	12.75	12.49	11.06	9.14	7.02	7.00	8.25	8.58	8.73	8.88	8.95	9.01
f/M_p	13	14	15	20	30	40	50	60	70	80	90	100
$\lg(g/\text{GeV})^{min}$	9.05	9.08	9.09	9.11	9.05	9.12	9.09	9.07	9.05	9.04	9.03	9.05

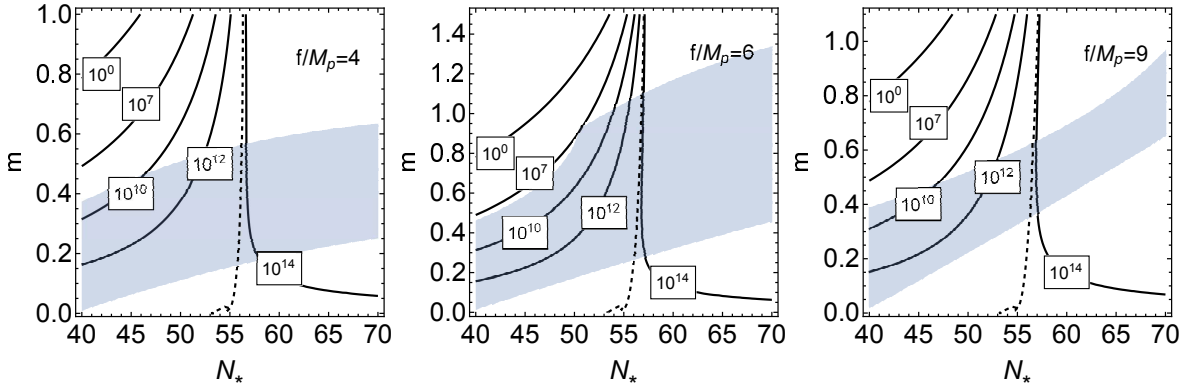


FIG. 9. The coupling constant g/GeV with respect to variables N_* and m corresponding to $f/M_p = 4, 6$ and 9 , respectively.

ACKNOWLEDGMENTS

We are deeply grateful to S.J. Wang for his helpful discussions and comments, especially to Prof. R.G. Cai and Prof. Z.K. Guo for their kindly help. This work is supported by the National Natural Science Foundation of China (Grant Nos. 11175077 and 11575075).

-
- [1] A. H. Guth, Phys. Rev. D **23**, 347 (1981).
[2] A. D. Linde, Phys. Lett. B **108**, 389 (1982).
[3] A. Albrecht, P. J. Steinhardt, Phys. Rev. Lett. **48**, 1220 (1982).
[4] S. W. Hawking, I. G. Moss, Phys. Lett. B **110**, 35 (1982).
[5] A. D. Linde, Phys. Lett. B **129**, 177 (1983).
[6] V. F. Mukhanov, G. Chibisov, JETP. Lett. **33**, 532 (1981).
[7] S. W. Hawking, Phys. Lett. B **115**, 295 (1982).
[8] A. H. Guth, S. Y. Pi, Phys. Rev. Lett. **49**, 1110 (1982).
[9] L. Boubekeur, D. H. Lyth, JCAP. **0507**, 010 (2005).
[10] K. Freese, J. A. Frieman, A. V. Olinto, Phys. Rev. Lett. **65**, 3233 (1990).
[11] F. C. Adams, J. R. Bond, K. Freese, J. A. Frieman, A. V. Olinto, Phys. Rev. D **47**, 426 (1993).
[12] R. Kallosh, A. Linde, JCAP. **1306**, 028 (2013).
[13] R. Kallosh, A. Linde, D. Roest, JHEP. **1311**, 198 (2013).
[14] A. R. Liddle, D. H. Lyth, Phys. Lett. B **291**, 391 (1992).
[15] A. R. Liddle, P. Parsons, J. D. Barrow, Phys. Rev. D **50**, 7222 (1994).
[16] P. J. Steinhardt, M. S. Turner, Phys. Rev. D **29**, 2162 (1984).
[17] R. G. Cai, Z. K. Guo, S. J. Wang, Phys. Rev. D **92**, 063506 (2015).
[18] Q. G. Huang, K. Wang, S. Wang, Phys. Rev. D **93**, 103516 (2016).
[19] J. Martin, C. Ringeval, V. Vennina, Phys. Dark Univ. **5-6**, 75 (2014).
[20] P. A. R. Ade, et al. (Keck Array and BICEP2 Collaborations), Phys. Rev. Lett. **116**, 031302 (2016).
[21] P. A. R. Ade, et al. (Planck Collaboration), Astron. Astrophys. **571**, A16 (2014).
[22] P. A. R. Ade, et al. (Planck Collaboration), Astron. Astrophys. **571**, A22 (2014).
[23] P. A. R. Ade, et al. (Planck Collaboration), Astron. Astrophys. **594**, A13 (2016).
[24] P. A. R. Ade, et al. (Planck Collaboration), Astron. Astrophys. **594**, A20 (2016).
[25] L. F. Abbott, E. Farhi, M. B. Wise, Phys. Lett. B **117**, 28 (1982).
[26] L. Kofman, A. D. Linde, A. A. Starobinsky, Phys. Rev. D **56**, 3258 (1997).
[27] R. Allahverdi, R. Brandenberger, F. Y. Cyr-Racine, A. Mazumdar, Ann. Rev. Nucl. Part. Sci **60**, 27 (2010).
[28] J. B. Munoz, M. Kamionkowski, Phys. Rev. D **91**, 043521 (2015).
[29] D. I. Podolsky, G. N. Felder, L. Kofman, and M. Peloso, Phys. Rev. D **73**, 023501 (2006).
[30] Y. Ueno, K. Yamamoto, Phys. Rev. D **93**, 083524 (2016).
[31] J. Martin, C. Ringeval, Phys. Rev. D **82**, 023511 (2010).
[32] L. Dai, M. Kamionkowski, J. Wang, Phys. Rev. Lett. **113**, 041302 (2014).
[33] S. Dodelson, *Modern Cosmology* (Academic Press, 2003).
[34] V. Mukhanov, *Physical Foundations of Cosmology* (Cambridge Universe Press, 2005).